



The open flux evolution of a solar-mass star on the main sequence

V. See,^{1,2★} M. Jardine,¹ A. A. Vidotto,³ J.-F. Donati,^{4,5} S. Boro Saikia,^{6,7} R. Fares,^{8,9}
C. P. Folsom,^{4,5,10,11} S. V. Jeffers,⁶ S. C. Marsden,¹² J. Morin,¹³ P. Petit^{4,5}
and the BCOOL Collaboration

¹*SUPA, School of Physics and Astronomy, University of St Andrews, North Haugh, St Andrews KY16 9SS, UK*

²*Department of Physics and Astronomy, Physics Building, University of Exeter, Stocker Road, Exeter EX4 4QL, UK*

³*School of Physics, Trinity College Dublin, University of Dublin, Dublin-2, Ireland*

⁴*Université de Toulouse, UPS-OMP, Institut de Recherche en Astrophysique et Planétologie, F-31400 Toulouse, France*

⁵*CNRS, Institut de Recherche en Astrophysique et Planétologie, 14 Avenue Edouard Belin, F-31400 Toulouse, France*

⁶*Universität Göttingen, Institut für Astrophysik, Friedrich-Hund-Platz 1, D-37077 Göttingen, Germany*

⁷*Institut für Astronomie, Universität Wien, Türkenschanzstrasse 17, A-1180 Wien, Austria*

⁸*INAF-Osservatorio Astrofisico di Catania, Via Santa Sofia, 78, I-95123 Catania, Italy*

⁹*Department of Natural Sciences, School of Arts and Sciences, Lebanese American University, PO Box 36, Byblos, Lebanon*

¹⁰*Univ. Grenoble Alpes, IPAG, F-38000 Grenoble, France*

¹¹*CNRS, IPAG, F-38000 Grenoble, France*

¹²*Computational Engineering and Science Research Centre, University of Southern Queensland, Toowoomba, 4350 Queensland (QLD), Australia*

¹³*Laboratoire Univers et Particules de Montpellier, Université de Montpellier, CNRS, F-34095 Montpellier, France*

Accepted 2017 October 4. Received 2017 September 29; in original form 2017 March 27

ABSTRACT

Magnetic activity is known to be correlated to the rotation period for moderately active main-sequence solar-like stars. In turn, the stellar rotation period evolves as a result of magnetized stellar winds that carry away angular momentum. Understanding the interplay between magnetic activity and stellar rotation is therefore a central task for stellar astrophysics. Angular momentum evolution models typically employ spin-down torques that are formulated in terms of the surface magnetic field strength. However, these formulations fail to account for the magnetic field geometry, unlike those that are expressed in terms of the open flux, i.e. the magnetic flux along which stellar winds flow. In this work, we model the angular momentum evolution of main-sequence solar-mass stars using a torque law formulated in terms of the open flux. This is done using a potential field source surface model in conjunction with the Zeeman–Doppler magnetograms of a sample of roughly solar-mass stars. We explore how the open flux of these stars varies with stellar rotation and choice of source surface radii. We also explore the effect of field geometry by using two methods of determining the open flux. The first method only accounts for the dipole component while the second accounts for the full set of spherical harmonics available in the Zeeman–Doppler magnetogram. We find only a small difference between the two methods, demonstrating that the open flux, and indeed the spin-down, of main-sequence solar-mass stars is likely dominated by the dipolar component of the magnetic field.

Key words: techniques: polarimetric – stars: activity – stars: evolution – stars: magnetic field – stars: rotation.

1 INTRODUCTION

Understanding how the angular momentum and rotation periods of low-mass stars ($M_{\star} \lesssim 1.3 M_{\odot}$) evolve over their lifetimes is an important goal within stellar astrophysics. For example,

rotation is known to be correlated to numerous forms of magnetic activity including X-ray emission (Pizzolato et al. 2003; Wright et al. 2011), chromospheric activity (Noyes et al. 1984; Mamajek & Hillenbrand 2008) and large-scale magnetic field generation (Petit et al. 2008; Vidotto et al. 2014b; See et al. 2015b; Folsom et al. 2016; See et al. 2016). The stellar rotation period can also be used as a proxy for the stellar age using the so-called gyrochronology relations (Barnes 2003, 2007, 2010), at least for stars whose rotation

* E-mail: w.see@exeter.ac.uk

periods have converged on to a single track in the rotation period–age plane (for solar-mass stars, convergence occurs at ~ 1 Gyr). Finally, the magnetic activity and rotation history of a host star can also have a significant impact on the potential habitability of exoplanets (Wood et al. 2014; Tu et al. 2015; Ribas et al. 2016; Gallet et al. 2017). For example, stellar winds can significantly compress planetary magnetospheres (Vidotto et al. 2013; See et al. 2014) and reduce their ability to protect the planetary atmosphere from the erosive effects of the wind. Planetary atmospheres can also be eroded away by photoevaporation caused by high-energy radiation (Lammer et al. 2003). The rate at which this occurs depends strongly on the initial rotation period of the host star (Johnstone et al. 2015b).

Along the main sequence, the main agent of angular momentum evolution is magnetized stellar winds that carry angular momentum away from the central star. Many authors have studied the rate at which stars lose angular momentum (Cohen & Drake 2014; Vidotto et al. 2014a; Garraffo, Drake & Cohen 2015; Nicholson et al. 2016; See et al. 2017) or formulated braking laws that describe how the angular momentum loss varies as a function of the parameters of the host star (Matt et al. 2012b; Reiners & Mohanty 2012; Réville et al. 2015a). These braking laws have subsequently been used to model stellar rotation period evolution from the pre-main sequence (PMS) to ages older than the Sun (Gallet & Bouvier 2013, 2015; Brown 2014; Johnstone et al. 2015a; Matt et al. 2015; Amard et al. 2016; Blackman & Owen 2016; van Saders et al. 2016).

Numerous studies have shown that the open flux is an important parameter in the context of angular momentum loss (Mestel & Spruit 1987; Vidotto et al. 2014a; Réville et al. 2015a,b). However, it is not directly observable and must be estimated using physical models. One such model is the potential field source surface (PFSS) model (Altschuler & Newkirk 1969). This model takes an input magnetogram of the stellar surface and extrapolates the field upwards to the so-called source surface; a spherical surface that represents the limit of coronal confinement. Once the source surface is reached, the field lines are assumed to be open and radial, mimicking the action of plasma pressure opening up closed field lines.

A number of factors can affect the amount of open flux estimated by the PFSS model. The first is the choice of an input magnetogram. Previous theoretical work has shown that, when considering individual field modes, stars with dipolar surface fields have the most open flux and that the open flux decreases with increasing spherical harmonic degree (quadrupole, octupole, etc.; Garraffo et al. 2015; Réville et al. 2015a). For stellar studies, the input magnetogram is typically a Zeeman–Doppler imaging (ZDI) map (Jardine, Collier Cameron & Donati 2002; Gregory et al. 2006; Fares et al. 2010; Lang et al. 2012; Johnstone et al. 2014; See et al. 2015a). ZDI is a tomographic technique that is capable of reconstructing the large-scale surface magnetic field structure of cool-dwarf stars (Semel 1989; Brown et al. 1991; Donati & Brown 1997; Donati et al. 2006). Over the last two decades, a considerable amount of effort has been dedicated to investigating the field geometry of low-mass stars. It has been found that their surface fields are composed of a mixture of spherical harmonic modes (e.g. Jeffers et al. 2014; Boro Saikia et al. 2015, 2016; Folsom et al. 2016). However, recent work suggests that the open flux is dominated by the dipolar component of the field, at least for the choice of source surface radius used in those works (Lang et al. 2014; Jardine, Vidotto & See 2017; See et al. 2017). This is because the dipolar component of the field decays the most slowly with height above the stellar surface. Given that the ZDI technique can typically reconstruct the stellar magnetic field up to a spherical harmonic mode of, at least, $\ell = 5$, ZDI maps

are an appropriate choice of inner boundary condition for the PFSS model in the context of determining the open flux.

The source surface radius is another parameter that can affect the amount of open flux recovered. Within the PFSS model, it is a free parameter but it is observationally unconstrained for stars other than our Sun. For a given input map, more of the flux is forced to be open for smaller values of the source surface radius. Additionally, if the source surface is sufficiently small, the higher order field modes may not have completely decayed away and may contribute towards the open flux. Typically, the source surface radius is picked to have values similar to the solar value ($\sim 2.5r_*$) but in reality it should vary as a function of the fundamental parameters of the star (Réville et al. 2015b).

In See et al. (2017), we studied how the open flux and the corresponding spin-down torque varied using a sample of low-mass stars with a wide range of masses and rotation periods. We found that the open flux of stars with Rossby numbers, Ro , greater than ~ 0.01 follows the classical activity rotation relation shape but that $Ro \lesssim 0.01$ stars departed from this relation. These results were obtained using the simplifying assumption that all the stars had source surface radii of $r_{ss} = 3.41r_*$. This is a useful assumption since it allows for a rapid assessment of how stellar open flux varies over a large portion of the HR diagram. However, it ignores the fact that the source surface radius likely varies as a function of mass and rotation period. Indeed, to these authors’ knowledge, there has not been a systematic study of how the source surface affects the open flux recovered for a set of realistic input magnetograms to date.

In this study, we will use a sample of 22 main-sequence stars of roughly solar mass ($0.9 M_\odot < M_* < 1.1 M_\odot$) which have had their large-scale surface magnetic fields mapped to investigate the open flux evolution main-sequence solar-mass stars. Using a PFSS model, we investigate how the open flux of these stars varies for different source surface radii and the effect of including/excluding higher order field modes. The angular momentum evolution of a solar-mass star can then be calculated over its lifetime using these open flux formulations, in conjunction with the braking law of Réville et al. (2015a). We use rotation period data from open clusters of known ages to constrain our angular momentum evolution model and determine how the source surface radius and open flux vary over the main-sequence lifetime. In Section 2, we outline the details of our spin-down model. In Section 3, we outline two methods of determining the open flux as a function of rotation and source surface radius. In Section 4, we discuss the open cluster data we use to calibrate our model. In Section 5, we present the results of our angular momentum evolution model. A discussion and the conclusions follow in Section 6.

2 ANGULAR MOMENTUM EVOLUTION MODEL

In order to determine how the rotation period of a star evolves, we need to solve the angular momentum equation,

$$\frac{d\Omega_*}{dt} = \frac{\dot{J}}{I_*} - \frac{\Omega_*}{I_*} \frac{dI_*}{dt}, \quad (1)$$

where $\Omega_* = 2\pi/P_{\text{rot}}$ is the stellar angular velocity, P_{rot} is the stellar rotation period, t is time, \dot{J} is the angular momentum-loss rate or spin-down torque and I_* is the moment of inertia of the star. For simplicity, we will assume solid body rotation throughout the entire main-sequence lifetime. We use the evolutionary models of Baraffe et al. (2015) for a solar-mass star to determine how the moment of inertia changes with time although we note that the internal structure

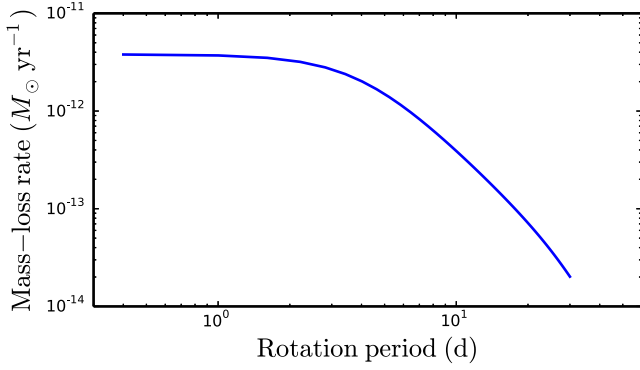


Figure 1. Mass-loss rate against rotation period for a solar-mass star as calculated using the model of Cranmer & Saar (2011).

of a star remains relatively constant on the main sequence and so the changes in angular velocity are dominated by the spin-down torque term in equation (1).

For the spin-down torque, we use the formulation of Réville et al. (2015a),

$$\dot{J}_{R15} = \dot{M} \Omega_* r_*^2 K_3^2 \left(\frac{\Upsilon_{\text{open}}}{(1 + f^2/K_4^2)^{1/2}} \right)^{2m}, \quad (2)$$

where \dot{M} is the mass-loss rate, r_* is the stellar radius, $\Upsilon_{\text{open}} = \Phi_{\text{open}}^2 / (r_*^2 \dot{M} v_{\text{esc}})$ is a measure of the magnetization of the open field lines, Φ_{open} is the open flux, $v_{\text{esc}} = (2GM_*/r_*)^{1/2}$ is the stellar escape velocity, M_* is the stellar mass, $f = \Omega_* r_*^{3/2} (GM_*)^{-1/2}$ is the angular rotation speed normalized to the breakup speed and $K_3 = 0.65$, $K_4 = 0.06$ and $m = 0.31$ are fit parameters determined from the results of magnetohydrodynamic (MHD) simulations.¹ We use the model of Cranmer & Saar (2011) to estimate the mass-loss rate. This is a 1D model that estimates the magnitude of the Alfvén wave energy flux generated by subsurface convective motions. The model tracks this energy flux through the stellar surface and estimates the amount that is deposited as heat in the transition region. It is this heat that is responsible for driving the winds in this model. Many previous studies have shown that magnetic activity scales with rotation. In the model of Cranmer & Saar (2011), this scaling is encapsulated by the magnetic filling factor that is estimated using empirical scaling relations based on previously published data. Fig. 1 shows the mass-loss rate of a solar-mass star as a function of rotation period using this model. Similarly to other phenomena related to magnetic activity, the mass-loss rate increases with decreasing rotation period and saturates at the fastest rotation periods. In order to estimate the open flux, we will use the PFSS model in conjunction with ZDI maps. Investigating how the open flux varies with rotation and source surface radii will form the focus of this work and will be presented in Section 3. Having calculated \dot{J}_{R15} , we will assume that the real spin-down torque is proportional to this value, i.e. $\dot{J} = k \dot{J}_{R15}$. Such an assumption has also been made in previous works (Gallet & Bouvier 2013, 2015; Johnstone et al. 2015a). We will fit for the proportionality constant, k , and discuss its physical significance in Section 5. Lastly, Table 1 contains the solar values that we use in this study.

¹ The value of K_3 is given as 1.4 by Réville et al. (2015a). However, this is a typographical error and the true value is $K_3 = 0.65$ (Réville, priv. comm.).

Table 1. Adopted solar values in this study.

M_{\odot} (solar mass)	2.0×10^{33} g
r_{\odot} (solar radius)	6.96×10^{10} cm
$P_{\text{rot},\odot}$ (solar rotation period)	26 d
τ_c (solar-mass convective turnover time)	14.45 d
$P_{\text{rot,crit}}$ (critical rotation period)	1.45 d
$r_{\text{ss},\odot}$ (solar source surface radius)	$2.5 r_{\odot}$
t_{\odot} (solar age)	4.6 Gyr

3 ESTIMATING THE OPEN FLUX

3.1 The PFSS model

In order to estimate the open flux, we use the PFSS model (Altschuler & Newkirk 1969). In this model, the magnetic field is assumed to be in a potential state, i.e. current free, and the three components are given by

$$B_r = - \sum_{l=1}^N \sum_{m=l}^l [a_{lm} r^{l-1} - (l+1) b_{lm} r^{-(l+2)}] P_{lm}(\cos \theta) e^{im\phi} \quad (3)$$

$$B_{\theta} = - \sum_{l=1}^N \sum_{m=l}^l [a_{lm} r^{l-1} + b_{lm} r^{-(l+2)}] \frac{d}{d\theta} P_{lm}(\cos \theta) e^{im\phi} \quad (4)$$

$$B_{\phi} = - \sum_{l=1}^N \sum_{m=l}^l [a_{lm} r^{l-1} + b_{lm} r^{-(l+2)}] P_{lm}(\cos \theta) \frac{im}{\sin \theta} e^{im\phi}, \quad (5)$$

where l is the spherical harmonic degree, m is the azimuthal number, a_{lm} and b_{lm} are the amplitudes of each spherical harmonic component and P_{lm} are the Legendre polynomials. Equations (3)–(5) only apply between the stellar surface and the source surface with the field assumed to decay radially as an inverse square law above the source surface. In order to determine the values of a_{lm} and b_{lm} , two boundary conditions are required. The first is the field geometry at the stellar surface which is set using ZDI maps. We use a sample of 22 main-sequence stars with masses between 0.9 and $1.1 M_{\odot}$.² The large-scale surface magnetic fields of each of these stars have been mapped with ZDI, sometimes over multiple epochs. The parameters of these stars are shown in Table 2 along with a reference to the article their magnetic map was originally published in. The stellar parameters are taken from the same references or Vidotto et al. (2014b) and references therein. It should be noted that values for the stellar parameters have been obtained from a number of different sources which will add systematic consistency errors. The second boundary condition is the requirement that the field must become purely radial at some distance away from the star known as the source surface radius, r_{ss} . As discussed in the introduction, the value of r_{ss} is a free parameter in this model. The open flux is then given by integrating the radial field over the source surface

$$\Phi_{\text{open}} = \oint_{r_{\text{ss}}} |B_r| dS. \quad (6)$$

² There are a number of reported masses for AB Dor in the literature. Donati, Collier Cameron & Petit (2003b) give its mass as $1 M_{\odot}$ which falls within our mass bracket ($0.9 M_{\odot} \leq 1 M_{\odot} \leq 1.1 M_{\odot}$). On the other hand, Guirado et al. (2010) report a dynamical mass of $0.86 M_{\odot}$. It is therefore unclear whether AB Dor should be included in our sample. We note that AB Dor falls into the saturated regime and is not included in any of the fits in this work. Its inclusion does not affect our final numerical results and it simply serves to show that the field flux values we obtain in the saturated regime are reasonable. We have therefore included it in this work.

Table 2. Parameters of the stars mapped with ZDI listed in an ascending order of rotation period: stellar mass, radius, rotation period, age, surface dipolar flux, total surface flux, and the source surface radius for which the open flux calculated using the multipolar method differs from the open flux calculated using the dipolar method by 10% (see Sections 3.2 and 3.3). No value is listed for stars for which the dipolar and multipolar open fluxes never differ by more than 10 percent. The observation epoch at which each star was observed and references for the paper in which the original magnetic map was published are also listed. The stellar parameters are also taken from these references or Vidotto et al. (2014b) and references therein.

Star ID	M_* (M_\odot)	r_* (r_\odot)	P_{rot} (d)	Age (Myr)	$\Phi_{*,\text{dip}}$ (10^{23} Mx)	Φ_* (10^{23} Mx)	$r_{\text{ss},10\%}$ (r_*)	Obs epoch	Ref.
AB Dor	1 ^a	1	0.51	120	34.65	79.76	1.84	2001 Dec	Donati et al. (2003a)
–	–	–	–	–	44.31	65.15	1.45	2002 Dec	–
PELS 031	0.95	1.05	2.5	125	4.90	11.65	2.51	2013 Nov	Folsom et al. (2016)
HII 296	0.9	0.93	2.61	125	25.72	27.69	–	2009 Oct	Folsom et al. (2016)
BD-16351	0.9	0.88	3.21	42	14.62	15.55	–	2012 Sept	Folsom et al. (2016)
HD 166435	1.04	0.99	3.43	3800	1.88	6.53	4.05	–	Petit et al. (in preparation)
HD 175726	1.06	1.06	3.92	500	2.40	4.71	2.11	–	Petit et al. (in preparation)
V 447 Lac	0.9	0.81	4.43	257	2.50	4.17	2.83	2014 Jun	Folsom et al. (2016)
HN Peg	1.085	1.04	4.6	260	6.05	7.06	1.33	2007 Jul	Boro Saikia et al. (2015)
–	–	–	–	–	2.96	4.65	1.76	2008 Aug	–
–	–	–	–	–	4.39	5.91	1.33	2009 Jun	–
–	–	–	–	–	5.44	7.30	1.29	2010 Jul	–
–	–	–	–	–	4.56	7.72	2.06	2011 Jul	–
–	–	–	–	–	8.17	9.46	1.13	2013 Jul	–
TYC 5164-567-1	0.9	0.89	4.68	120	22.57	23.51	–	2013 Jun	Folsom et al. (2016)
HD 39587	1.03	1.05	4.83	500	2.75	6.64	2.18	–	Petit et al. (in preparation)
HIP 12545	0.95	1.07	4.83	24	40.75	45.62	1.06	2012 Sept	Folsom et al. (2016)
HD 72905	1	1	5	500	1.90	4.57	3.23	–	Petit et al. (in preparation)
DX Leo	0.9	0.81	5.38	257	7.85	8.48	–	2014 May	Folsom et al. (2016)
V 439 And	0.95	0.92	6.23	257	4.31	4.51	–	2014 Sept	Folsom et al. (2016)
HD 190771	0.96	0.98	8.8	2700	2.84	3.98	2.09	–	Petit et al. (in preparation)
κ Ceti	1.03	0.95	9.3	600	4.38	6.23	1.85	2012 Oct	do Nascimento et al. (2016)
HD 73350	1.04	0.98	12.3	510	1.69	3.44	2.84	–	Petit et al. (in preparation)
HD 73256	1.05	0.89	14	830	1.21	2.12	2.66	2008 Jan	Fares et al. (2013)
HD 56124	1.03	1.01	18	4500	1.11	1.12	–	–	Petit et al. (in preparation)
18 Sco	0.98	1.02	22.7	4700	0.42	0.62	2.26	2007 Aug	Petit et al. (2008)
HD 9986	1.02	1.04	23	4300	0.33	0.34	–	–	Petit et al. (in preparation)
HD 46375	0.97	0.86	42	5000	0.81	0.83	–	2008 Jan	Fares et al. (2013)

Note. ^aWe have listed the mass for AB Dor as $1 M_\odot$ but there have been a range of reported masses for AB Dor in the literature. See the footnote in Section 3.1 for further discussion.

See et al. (2017) showed that for low-mass stars ($<1.4 M_\odot$), the open flux is determined predominantly by the dipolar component of the magnetic field, at least for their chosen source surface radii of $r_{\text{ss}} = 3.41 R_*$. In this work, we will investigate whether this assumption holds for different choices of the source surface radii. We will outline two methods of estimating the open flux of a solar-mass star. The first method will use only the dipolar component of the ZDI maps as inputs to the PFSS model while the second method will use the full set of spherical harmonics available in ZDI maps. We will refer to these as the dipolar and the multipolar methods, respectively.

3.2 Dipolar method of determining open flux

Fig. 2 shows the surface flux associated with the dipolar component ($l = 1$) of the ZDI maps, $\Phi_{*,\text{dip}}$, as a function of rotation period. In this work, we will define the unsaturated regime to be $\text{Ro} > 0.1$. For solar-mass stars, which have convective turnover times of 14.45 d (calculated using equation 11 of Wright et al. 2011), this corresponds to a critical rotation period of $P_{\text{rot,crit}} = 1.45$ d. The fit to the unsaturated stars (those stars with $P_{\text{rot}} > P_{\text{rot,crit}}$) has the form $\Phi_{*,\text{dip}} = (6.69 \pm 3.28) \times 10^{24} P_{\text{rot}}^{-1.58 \pm 0.23}$. This fit, as well as the others in this work, was done using the bisector ordinary least-squares method (Isobe et al. 1990). The errors on the fit are determined by considering only the scatter of the

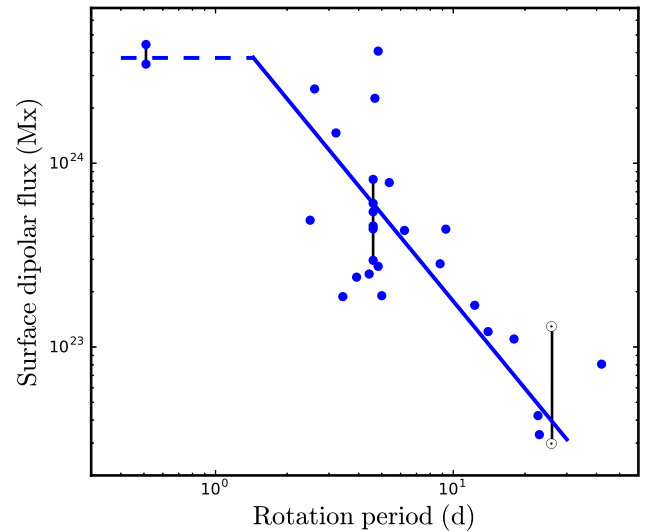


Figure 2. Surface dipolar flux against rotation period. Stars observed at multiple epochs are connected by a vertical line. The fit to the stars in the unsaturated regime (solid blue line, $P_{\text{rot}} > 1.44$ d) has the form $\Phi_{*,\text{dip}} = (6.69 \pm 3.28) \times 10^{24} P_{\text{rot}}^{-1.58 \pm 0.23}$. The surface dipolar flux has a value of 3.72×10^{24} Mx in the saturated regime (dashed blue line, $P_{\text{rot}} < 1.44$ d). Two solar symbols indicate the typical variation of the surface dipolar flux over the solar cycle (values are taken from Jardine et al. 2017).

points. From the presently available data, it is difficult to constrain the value of the surface dipolar flux in the saturated regime. Currently, only a single star of roughly solar mass in the saturated regime (AB Dor) has been mapped with ZDI. For now, we will assume that the surface dipolar flux transitions continuously from the unsaturated regime to the saturated regime such that it has a value of $6.69 \times 10^{24} P_{\text{rot,crit}}^{-1.58} = 3.72 \times 10^{24}$ Mx. This corresponds well with the surface dipolar flux of AB Dor. However, further ZDI observations of solar-mass stars in the saturated regime will be required to determine if this estimate of dipolar flux in the saturated regime is a representative of the true value.

In general, equations (3) and (6) should be used to calculate the open flux when using all the available spherical harmonics in a ZDI map. However, when considering only the dipolar component of the ZDI map, the open-to-surface flux ratio is simply given by

$$\frac{\Phi_{\text{open,dip}}}{\Phi_{\star,\text{dip}}} = \frac{3\tilde{r}_{\text{ss}}^2}{2\tilde{r}_{\text{ss}}^3 + 1}, \quad (7)$$

where $\tilde{r}_{\text{ss}} = r_{\text{ss}}/r_{\star}$ is the ratio of the source surface radii to the stellar radii. This simple expression exists because we are dealing with only a single spherical harmonic mode and no cross-terms arise when calculating the integral in equation (6). A full derivation of equation (7) is available in Appendix A. By combining equation (7) with the expression for the surface dipolar flux, as a function of rotation period, derived from Fig. 2, we have a simple way of estimating the dipolar open flux of a star as a function of rotation period and source surface radii. In this work, we will assume that the source surface radius can be parametrized as

$$r_{\text{ss}} = r_{\text{ss},\odot} \left(\frac{P_{\text{rot}}}{P_{\text{rot},\odot}} \right)^n, \quad (P_{\text{rot}} > P_{\text{rot,crit}})$$

$$r_{\text{ss}} = r_{\text{ss},\odot} \left(\frac{P_{\text{rot,crit}}}{P_{\text{rot},\odot}} \right)^n, \quad (P_{\text{rot}} < P_{\text{rot,crit}}), \quad (8)$$

where values for the solar source surface radius, $r_{\text{ss},\odot}$, and rotation period, $P_{\text{rot},\odot}$, can be found in Table 1 and n is a power-law index that we will determine in Section 5. In principle, to properly determine the source surface radius, one should consider the location where the plasma thermal pressure and bulk ram pressure of the wind are able to overcome the magnetic pressure of the field causing the field lines to open up (see Réville et al. 2015b for an in-depth discussion of how to determine the source surface radius). However, we choose to use the simplified form presented in equation (8). Such a dependence is not unreasonable given that many phenomena associated with stellar activity, such as large-scale magnetic fields (Vidotto et al. 2014b; See et al. 2015b), mass loss (Cranmer & Saar 2011) and X-ray emission (Wright et al. 2011), have a power-law dependence on rotation in the unsaturated regime with saturation occurring for the fastest rotators. It should also be noted that the source surface radius of a given star should vary due to various forms of intrinsic variability in the stellar magnetic field such as stellar cycles. These short-term fluctuations are not considered by our model and the value calculated using equation (8) should be regarded as a source surface radius value averaged over evolutionary time-scales.

3.3 Multipolar method of determining open flux

In this section, we will estimate the open flux using the full set of spherical harmonics available from the ZDI maps. Unfortunately, there is no simple analytic method of estimating the open flux from the surface flux analogous to equation (7) due to the summation

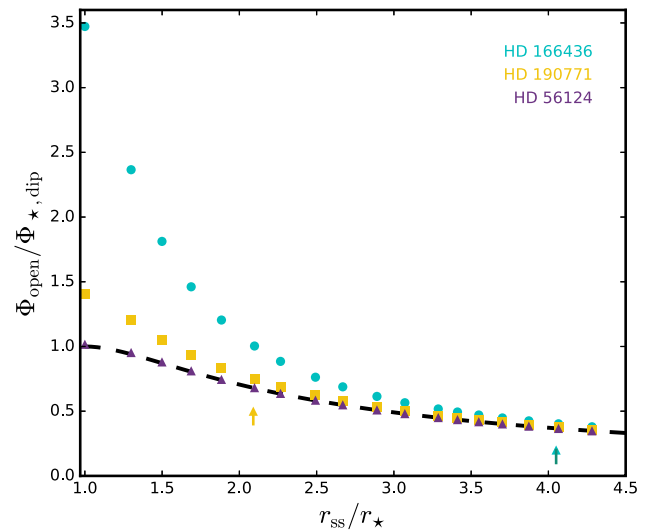


Figure 3. Open flux normalized to the surface dipolar flux against source surface radii for HD 166435 (cyan circles), HD 190771 (yellow squares) and HD 56124 (purple triangles). At $r_{\text{ss}}/r_{\star} = 1$, the open flux is equal to flux at the stellar surface since all the magnetic flux is forced to be open. The dashed line represents the normalized open flux from a purely dipolar field, i.e. equation (7). Cyan and yellow arrows indicate the $r_{\text{ss},10\%}$ values for HD 166435 and HD 190771. No arrow is shown for HD 56124 since the discrepancy between the open fluxes determined from the multipolar case and the dipolar case never exceeds 10 per cent.

over different modes in equation (3). We must therefore numerically evaluate equation (6) for a range of source surface radii to determine the impact of the higher order modes on the open flux. Fig. 3 shows the open flux, Φ_{open} , normalized to the surface dipolar flux, $\Phi_{\star,\text{dip}}$, against source surface radius for three stars from our sample. A dashed line represents the open flux expected in a purely dipolar case, i.e. as calculated by equation (7). The three chosen stars represent three cases. The surface magnetic field of HD 56124 (purple triangles), as determined from ZDI, is strongly dipolar. As such, it follows the pure dipole case (dashed line) very closely. On the other hand, the dipolar component represents only a small fraction of the magnetic energy in the ZDI map of HD 166435 (cyan circles). This star therefore shows large deviations from the pure dipole case at the smallest values of r_{ss} . HD 190771 (yellow squares) represents an intermediate case and is also a representative of the majority of the stars in our sample. From Fig. 3, it is clear to see why See et al. (2017) found that the dipole component dominated the open flux for their chosen source surface radii of $r_{\text{ss}} = 3.41r_{\star}$. Even for HD 166435, which has one of the weakest dipole components in our sample, the effects of higher order spherical harmonics have become small by $r_{\text{ss}} = 3.41r_{\star}$. In Table 2, we list $r_{\text{ss},10\%}$ values for each star. This is the source surface radius at which the discrepancy between the open flux calculated using the full set of spherical harmonic modes and the open flux calculated considering just the dipolar mode exceeds 10% (no value is listed if it never exceeds 10%). We also indicate the $r_{\text{ss},10\%}$ values for HD 166435 and HD 190771 with cyan and yellow arrows in Fig. 3, respectively. The choice of 10% is arbitrary but serves to illustrate how dominant the dipolar mode is for each star. In most cases, the discrepancy between the two methods only exceeds 10% at relatively small r_{ss} values; less than $2r_{\star}$ for the majority of our sample and less than $3r_{\star}$ for all but two stars.

In order to determine the effect of using the full spherical harmonic decomposition available in the ZDI maps rather than just the

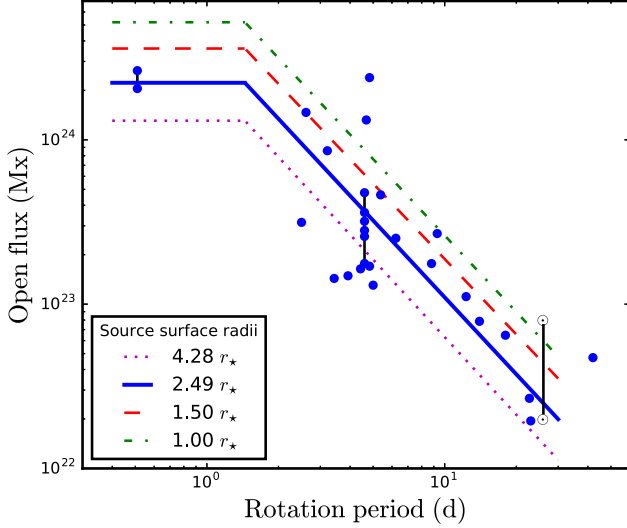


Figure 4. Open flux against rotation period calculated using $r_{ss} = 2.49r_*$ (blue circles). Stars observed at multiple epochs are connected by a vertical line. A fit to these points is shown with a solid blue line. Fits to the open flux calculated using $r_{ss} = 1.00r_*$, $1.50r_*$ and $4.28r_*$ are also shown. The data points for these fits are translated vertically in the plot when compared to the $r_{ss} = 2.49r_*$ data points and show a similar level of dispersion. However, they are not plotted for clarity. The coefficients for these fits, as well as other fits using different r_{ss} values, can be found in Table 3. Two solar symbols indicate the variation of the open flux over the solar cycle.

dipole components, we require a method of estimating the open flux as a function of rotation period and source surface radius. This is done as follows. First, we calculate the open flux of all the stars in our sample for a discrete set of different source surface radii, $r_{ss,i}$, in the range $1r_* - 4.28r_*$. Here, i is an index labelling the different source surface radii in this discrete set. For each of the source surface radii, $r_{ss,i}$, we perform a fit to the unsaturated stars, similarly to the one undertaken in Section 3.2, of the form $\Phi_{\text{open},i} = 10^{c_i} P_{\text{rot}}^{m_i}$, where m_i and c_i are fit parameters. As in Section 3.2, the saturated value of the open flux is taken to be $10^{c_i} P_{\text{rot,crit}}^{m_i}$. In Fig. 4, we show the open flux values for one choice of the source surface radii, $r_{ss,i} = 2.49r_*$ (blue points) as well as the fit to these points (solid blue line). This is the typical source surface radius chosen when studying the Sun. The PFSS model predicts solar open fluxes between $\sim 2 \times 10^{22}$ and $\sim 8 \times 10^{22}$ Mx (Jardine et al. 2017). For a solar rotation period, we predict an open flux of 2.5×10^{22} Mx using our fit, in good agreement with the solar values. Additionally, we also show the fits for three other choices of $r_{ss,i}$ to illustrate the impact of $r_{ss,i}$ on the fits. The data points for these fits are not shown for clarity. A full list of m_i and c_i coefficients for all values of $r_{ss,i}$ are available in Table 3.

Table 3. For a range of source surface radii, $r_{ss,i}$, we perform a fit of the form $\Phi_{\text{open},i} = 10^{c_i} P_{\text{rot}}^{m_i}$ to the unsaturated stars. Here, we list the m_i and c_i values for each $r_{ss,i}$.

$r_{ss,i}/r_*$	1.00	1.30	1.50	1.69	1.88	2.10
m_i	-1.545 ± 0.200	-1.522 ± 0.206	-1.525 ± 0.211	-1.533 ± 0.215	-1.540 ± 0.217	-1.547 ± 0.219
c_i	24.96 ± 0.18	24.86 ± 0.19	24.80 ± 0.20	24.75 ± 0.20	24.71 ± 0.20	24.67 ± 0.21
$r_{ss,i}/r_*$	2.27	2.49	2.67	2.89	3.07	3.29
m_i	-1.551 ± 0.221	-1.554 ± 0.222	-1.557 ± 0.222	-1.559 ± 0.223	-1.561 ± 0.223	-1.563 ± 0.224
c_i	24.63 ± 0.21	24.60 ± 0.21	24.57 ± 0.21	24.53 ± 0.21	24.51 ± 0.21	24.48 ± 0.21
$r_{ss,i}/r_*$	3.41	3.55	3.70	3.87	4.07	4.28
m_i	-1.564 ± 0.224	-1.565 ± 0.224	-1.566 ± 0.224	-1.566 ± 0.224	-1.567 ± 0.225	-1.568 ± 0.225
c_i	24.46 ± 0.21	24.45 ± 0.21	24.43 ± 0.21	24.41 ± 0.21	24.39 ± 0.21	24.37 ± 0.21

To calculate the open flux for an arbitrary P_{rot} and r_{ss} , we pick the two $r_{ss,i}$ values from Table 3 which bound our choice of r_{ss} . Using the m_i and c_i values associated with these two $r_{ss,i}$ values, we calculate two open flux values at the rotation period of interest, i.e. $\Phi_{\text{open},i} = 10^{c_i} P_{\text{rot}}^{m_i}$. Lastly, we interpolate between these two $\Phi_{\text{open},i}$ values to determine the open flux for our chosen r_{ss} . When calculating the open flux using a $r_{ss} > 4.28r_*$, the dipolar term strongly dominates (see Fig. 3) and we simply use equation (7).

4 OPEN CLUSTER DATA

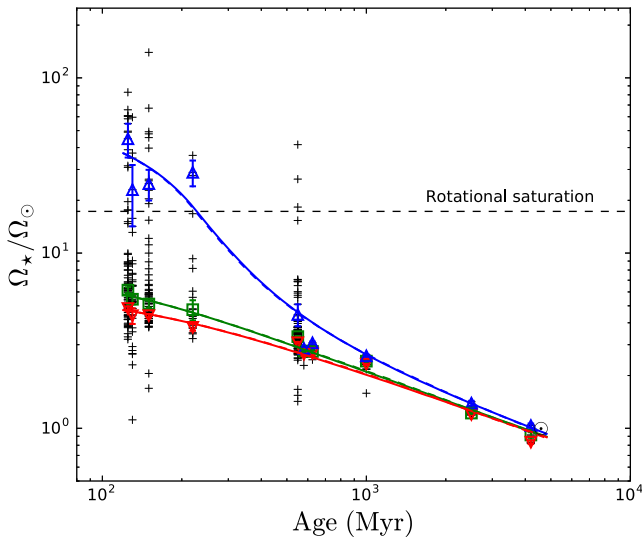
In order to constrain our model, we use the rotation periods of stars in open clusters of known ages. Since we are studying rotation period evolution on the main sequence, we have chosen clusters that have ages of 125 Myr or greater. In recent years, rotation period measurements in clusters older than 1 Gyr have been possible thanks to the *Kepler Space Telescope* (Meibom et al. 2015; Barnes et al. 2016). In particular, rotation period measurements from the 4 Gyr cluster M67 confirm that the Sun has a typical rotation period for a star of its age and mass (Barnes et al. 2016). The clusters we have used in this work and their ages are listed in Table 4. For each cluster, we will consider all the stars with masses between 0.9 and $1.1 M_{\odot}$ to be a representative of solar-mass stars. Fig. 5 shows the distribution of rotation periods for these stars in each of the clusters as a function of age (plotted with grey plus symbols) as well as our rotational evolution tracks (these will be discussed in Section 5). We can see that the rotation period distributions evolve with time. At early ages (< 200 Myr), solar-mass stars can have a large range of rotation periods with the fastest spinning nearly 100 times faster than the Sun. However, after ~ 1 Gyr, the rotation periods have nearly all converged on to a single valued track regardless of their rotational history. Similar to previous studies (Gallet & Bouvier 2013, 2015; Johnstone et al. 2015a), we will fit our model to the 25th, 50th and 90th percentiles of the rotation period distributions in each cluster. Implicit in this method is the assumption that a star at a given percentile will remain at that percentile throughout its entire evolution. We use a bootstrapping method to determine the rotation period at these percentiles for each cluster, as well as their errors. These are listed for each cluster in Table 4. They are also plotted with red downwards triangles (25th percentile), green squares (50th percentile) and blue upwards triangles (90th percentile) in Fig. 5.

5 THE ROTATION EVOLUTION OF A SOLAR-MASS STAR

In this section, we will fit rotation evolution tracks to the 90th, 50th and 25th percentiles in each of the open clusters. We will refer to these as the fast, intermediate and slow tracks, respectively. In

Table 4. The open cluster data used in this study. For each cluster, we list the age as well as the 25th, 50th and 90th percentiles of the angular velocity distribution of \sim solar-mass stars.

Cluster name	Age (Myr)	Ω_{25} (Ω_{\odot})	Ω_{50} (Ω_{\odot})	Ω_{90} (Ω_{\odot})	Ref.
Pleiades	125	4.83 ± 0.14	6.14 ± 0.24	44.91 ± 9.63	Hartman et al. (2010)
M50	130	4.39 ± 0.46	5.45 ± 0.34	23.01 ± 8.67	Irwin et al. (2009)
M35	150	4.39 ± 0.10	5.12 ± 0.23	24.90 ± 4.90	Meibom, Mathieu & Stassun (2009)
M34	220	3.77 ± 0.17	4.75 ± 0.63	28.89 ± 4.74	Meibom et al. (2011b)
M37	550	3.08 ± 0.04	3.34 ± 0.03	4.46 ± 0.67	Hartman et al. (2009)
Praesepe	580	2.64 ± 0.05	2.76 ± 0.04	2.85 ± 0.03	Delorme et al. (2011)
Hyades	625	2.68 ± 0.07	2.75 ± 0.06	3.07 ± 0.05	Delorme et al. (2011)
NGC 6811	1000	2.32 ± 0.02	2.42 ± 0.02	2.59 ± 0.05	Meibom et al. (2011a)
NGC6819	2500	1.20 ± 0.01	1.22 ± 0.01	1.39 ± 0.05	Meibom et al. (2015)
M67	4200	0.83 ± 0.02	0.92 ± 0.03	1.04 ± 0.03	Barnes et al. (2016)

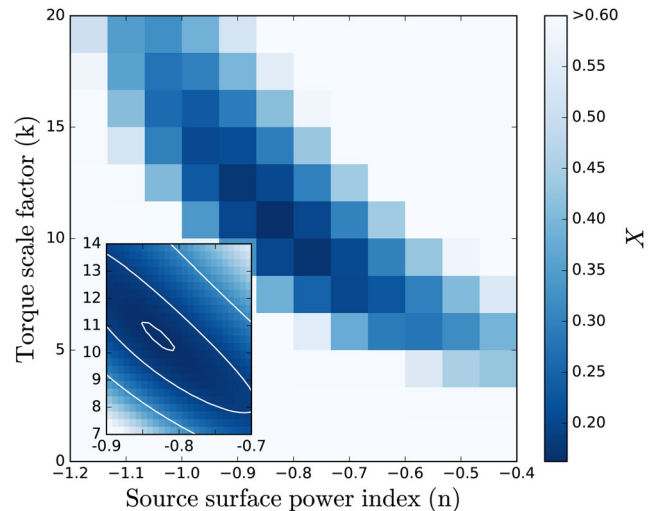
**Figure 5.** The rotation evolution of a solar-mass star. Plus symbols indicate the observed rotation periods of solar-mass stars in open clusters. Blue upwards triangles, green squares and red downwards triangles represent the 90th, 50th and 25th percentile in each of the clusters, respectively. The blue, green and red tracks show the rotation evolution of a fast, intermediate and slow solar-mass star as calculated with the dipole method (solid lines) and the multipolar method (dashed lines). The horizontal dashed line indicates the saturation threshold. Data and references for the cluster data can be found in Table 4.

order to determine the best-fitting values for the power-law index of the source surface radii scaling, n , and the scaling constant used to determine the spin-down torque, k , we require a goodness-of-fit parameter. We will use

$$X = \sum_j (\log \Omega_{\text{obs},j} - \log \Omega_{\text{model},j})^2. \quad (9)$$

Here, $\Omega_{\text{obs},j}$ refers to the observed angular velocities from open clusters and $\Omega_{\text{model},j}$ refers our model's estimate of $\Omega_{\text{obs},j}$. The summation over the index, j , is performed over the 25th, 50th and 90th percentiles for every cluster as shown in Table 4. This is a similar goodness-of-fit parameter to that used by Johnstone et al. (2015a). However, unlike these authors, we do not assign different weights to the different clusters. Tests indicate that giving older clusters a larger weighting does not significantly change our results.

In Fig. 6, we calculate the value of X over a grid of n and k values using the dipole method of determining the open flux (as described in Section 3.2). There is a well-defined minimum in X which occurs

**Figure 6.** The goodness-of-fit parameter, X , calculated over a grid of source surface power indices, n , and torque scalefactors, k , for the dipolar method. X values larger than 0.6 have been truncated to 0.6. The inset shows a higher resolution search through the n and k values around the minima. Contours for $X = \{0.16, 0.19, 0.3\}$ are also shown on the inset. The minimum in X occurs at $n_{\text{dip}} = -0.84$ and $k_{\text{dip}} = 10.64$.

at $n_{\text{dip}} = -0.84$ and $k_{\text{dip}} = 10.64$. It is worth noting that some degeneracy exists between n_{dip} and k_{dip} however. A more (less) negative value of n_{dip} can be partially offset by a larger (smaller) k_{dip} value for only a small increase in our goodness-of-fit parameter. Using n_{dip} and k_{dip} , we calculate the fast, intermediate and slow tracks that are plotted with solid red, green and blue lines in Fig. 5. By combining equations (7) and (8) with the fit from Fig. 2 and the value of n_{dip} , we can also determine the functional dependence of the open flux on the rotation period in our model. This is given by

$$\Phi_{\text{open,dip}} = 7.27 \times 10^{23} \frac{\tilde{P}_{\text{rot}}^{-3.26}}{31.3 \tilde{P}_{\text{rot}}^{-2.52} + 1}, \quad (P_{\text{rot}} > P_{\text{rot,crit}})$$

$$\Phi_{\text{open,dip,sat}} = 2.00 \times 10^{23}, \quad (P_{\text{rot}} < P_{\text{rot,crit}}), \quad (10)$$

where $\tilde{P}_{\text{rot}} = P_{\text{rot}}/P_{\text{rot},\odot}$.

The fact that $k_{\text{dip}} = 10.64$ has a value that is greater than 1 suggests that we are underestimating the spin-down torque in some way. This could be attributed to a number of reasons. For instance, the coronal temperature, a parameter that is kept fixed in the simulations of Réville et al. (2015a), can affect the rate at which angular momentum is lost from a star, even for a fixed mass-loss rate

(Pantolmos & Matt 2017). Additionally, the mass-loss rates we use may be systematically underestimated causing a lower than expected spin-down torque. It is worth emphasizing that mass-loss rates are extremely difficult to estimate and poorly constrained observationally. Differences between the mass-loss rate estimated by the model of Cranmer & Saar (2011) and the real mass-loss rates of stars could be absorbed into the fit parameter k (and perhaps n). Currently, there is no way of determining how much of the fact that k_{dip} is larger than 1 can be attributed to inaccurately estimating mass-loss rates. Although the mass-loss rates predicted by the model of Cranmer & Saar (2011) agree reasonably well with observations of the Sun, they may be less accurate for younger or more rapidly rotating stars. Lastly, we have assumed solid body rotation for simplicity. However, if core-envelope decoupling were included, the stellar wind braking should be more efficient since it would be acting on the envelope only. This should reduce the value of k_{dip} which we obtain with our model. Johnstone et al. (2015a) obtain a torque scaling value of 11 within their model which is comparable to our value. However, Gallet & Bouvier (2015) obtained a value of 1.7 in their solar-mass models which suggests their models may be capturing the relevant physics more accurately.

It is also worth noting that the particular values of n_{dip} and k_{dip} we obtain are dependent on the form of the flux–rotation relation that we adopt, i.e. the fit from Fig. 2. For example, if we only fit to the stars in Fig. 2 with masses $0.95 M_{\odot} \leq M_{\star} \leq 1.05 M_{\odot}$, we recover $n_{\text{dip}} = -0.67$ and $k_{\text{dip}} = 8.25$. It is clear that more ZDI observations of solar-mass stars are needed in order to refine our model. For the remainder of this work, we will consider the canonical n_{dip} and k_{dip} values to be those determined using the full ZDI sample, i.e. the stars with masses $0.9 M_{\odot} \leq M_{\star} \leq 1.1 M_{\odot}$ since this matches the mass bin width chosen for the open cluster rotation period data.

We perform this procedure again but using the multipolar method to determine the open flux (as described in Section 3.3). The equivalent plot of Fig. 6 for the multipolar method looks very similar (not shown) with a minimum in X occurring at $n_{\text{multi}} = -0.82$ and $k_{\text{multi}} = 10.18$. These values are similar to those calculated using the dipole-only method. Using the multipolar method of determining the open flux in conjunction with the n_{multi} and k_{multi} values, we plot the fast, intermediate and slow rotator tracks in Fig. 5 with dashed lines. The dashed rotation tracks lay almost exactly on the top of the solid rotation tracks determined using the dipolar method.

In Figs 7a and 7b, we plot the open flux and angular momentum-loss rate for both the dipolar and multipolar methods. The open flux and angular momentum-loss rates are both monotonically decreasing functions of age for the fast, intermediate and slow tracks. However, the fast tracks show a change in behaviour at ~ 200 Myr. As can be seen in Fig. 5, this is the age at which fast track stars transition from the saturated to the unsaturated regime. Unlike the fast track, stars on the intermediate and slow tracks are never rotating quickly enough to be in the saturated regime.

To understand why the two methods produce such similar results, we need to understand how the source surface radius evolves over the main sequence. Fig. 7c shows the source surface radius evolution for the fast, intermediate and slow tracks. These are calculated using equation (8) in conjunction with the rotation evolution tracks shown in Fig. 5 and our best-fitting values for n_{dip} and n_{multi} . Over the course of the main sequence, the source surface radii of these stars shrink as the star spins down and magnetic activity declines. For the intermediate and slow rotators, the source surface radius steadily drops from $\sim 10r_{\star}$ at ~ 100 Myr to $\sim 2.5r_{\star}$ by the age of the Sun. However, the fast rotator is spinning rapidly enough during its early main-sequence lifetime that its source surface radius attains

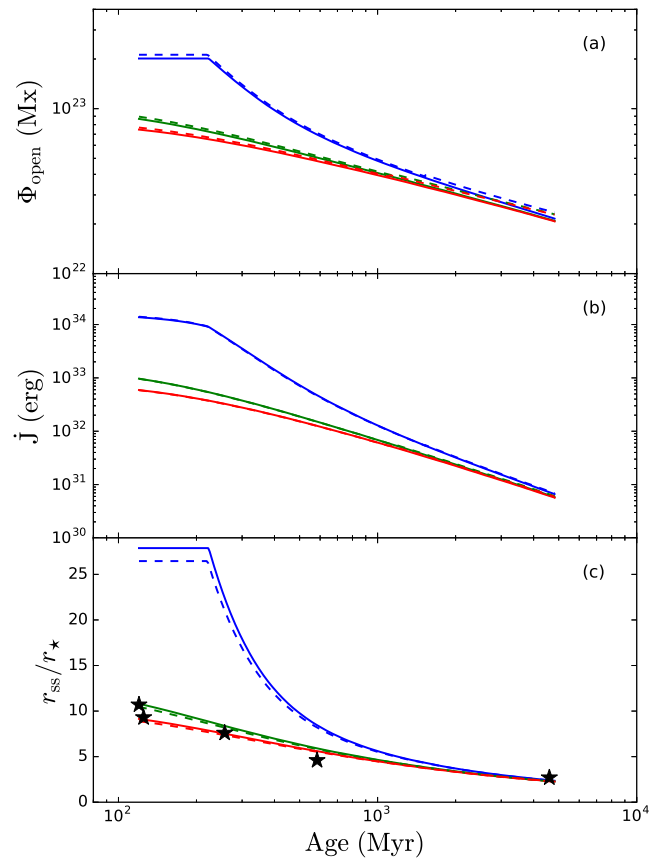


Figure 7. (a) Open flux, (b) angular momentum-loss rate and (c) source surface radii against age. In each panel, tracks are shown for fast (blue), intermediate (green) and slow (red) rotators calculated using the dipolar (solid lines) and multipolar (dashed lines) methods. In panel (c), the optimal source surface radii for a number of roughly solar-mass stars, as determined by Réville et al. (2016), are shown with star symbols (see the text).

the saturation value of $\sim 25r_{\star}$. Indeed, no solar-mass star can have a source surface radius larger than the saturation value under this model. From Fig. 3 and Table 2, we see that, for the majority of the stars in our sample, large differences in the open flux obtained from the dipolar and multipolar methods only occur at source surface radii smaller than roughly two or three stellar radii. Since all three tracks (and the tracks for any other percentile one might calculate) maintain source surface radii larger than $2.5r_{\star}$ until the age of the Sun, it should be a no surprise that there is very little difference between the dipolar and multipolar methods for calculating the open flux in the range of ages we have studied here. If we were to extend the rotation tracks to ages significantly past the age of the Sun, it is possible that the source surface radii would become small enough for the differences between the two methods of calculating the open flux to matter. However, currently, the rotation period behaviour of stars much older than the Sun is unclear. We will discuss this issue further in Section 6.

In Fig. 7c, we also plot the optimum source surface for a number of stars as estimated by Réville et al. (2016). These authors used 3D MHD simulations to study a sample of stars that are all roughly solar mass, using ZDI maps as a boundary condition for the magnetic field at the stellar surface. Their sample consisted of the stars BD-16351, TYC 5164-567-1, HII 296, DX Leo and AV 2177. The majority of these stars are also in our own sample. From their MHD simulations, they were able to determine the open flux of

each star. They then modelled each star with a PFSS model and determined the source surface radius that would be required for the PFSS model to produce the same open flux as their MHD models. These optimum source surface radii are plotted in Fig. 7c with star symbols. We can compare the optimum source surface radii of Réville et al. (2016) to the source surface radii as estimated by our own model. Taking $n_{\text{multi}} = -0.82$ from our multipolar method, we predict source surface radii of $13.5r_*$, $10.1r_*$, $16.4r_*$, $9.0r_*$ and $6.3r_*$ for BD-16351, TYC 5164-567-1, HII 296, DX Leo and AV 2177, respectively. The optimum source surface radii that Réville et al. (2016) predict are $8.1r_*$, $10.7r_*$, $9.3r_*$, $7.6r_*$ and $4.6r_*$. We see that our estimates are close to those of Réville et al. (2016) but our model tends to produce source surface radii that are larger, sometimes by a factor of ~ 1.7 . It is worth pointing out that the stars modelled by Réville et al. (2016) are all slow/moderate rotators. Our model predicts that the source surface radii of slowly/moderately rotating stars only change by a factor of a few. A similar study to that of Réville et al. (2016) modelling stars on the rapidly rotating track, where the source surface radii appear to change much more drastically over the main sequence in our model, would provide a much more stringent comparison.

Lastly, it is worth commenting on the source surface radii values. Our model estimates that the fastest rotators have $r_{\text{ss}} > 25r_*$ which is an order of magnitude larger than the Sun's source surface radii. Our simplified model requires that the source surface radii be this large for the fastest rotators but it is not clear whether, in reality, closed field loops can be maintained out to such a large distance. For instance, magnetocentrifugal forces acting on the coronal plasma may cause closed loops to open up closer to the stellar surface than they otherwise would have. Since our model does not self-consistently model the interactions between the stellar wind plasma and magnetic field, it is not possible to say how large an effect this might have. Such questions are left to future investigations and will require more sophisticated modelling of the relevant physics to answer.

6 DISCUSSION AND CONCLUSIONS

In this work, we have used a PFSS model, in conjunction with a sample of ZDI maps, to analyse how the open flux of solar-mass stars varies as a function of rotation and source surface radius. We then use these open flux relationships and the braking law of Réville et al. (2015a) to model the rotation period evolution of solar-mass stars on the main sequence up to the age of the Sun. We have assumed solid body rotation for simplicity. Within the PFSS model, the source surface radius is a free parameter. Previous works using this model have typically set the source surface radius to a value close to the solar value ($\sim 2.5r_*$). However, in this work, using rotation period data from open clusters, we are able to constrain how the source surface radius varies with the rotation period of the star. We predict that the fastest rotators begin life on the main sequence with a source surface radius of $\sim 26r_*$, while the intermediate and slower rotators start out with a source surface radius of $\sim 10r_*$. Eventually, the source surface radii of solar-mass stars will converge and reach the solar source surface radius by the age of the Sun.

Previous rotation period evolution models have typically used braking laws that are formulated in terms of the dipolar surface magnetic field strength (e.g. Matt et al. 2012b). However, we use the braking law of Réville et al. (2015a), which is formulated in terms of the open flux. In principle, this braking law allows us to account for higher order spherical harmonic modes in the surface magnetic

field. In practice, however, we find that the dipole component of the magnetic field dominates the open flux for all but the smallest choices of the source surface radius. As outlined in Section 5, the dipolar open flux in our model can be analytically calculated as a function of rotation period by combining equations (7) and (8) with the fit from Fig. 2.

When considering the effect of field geometry on angular momentum evolution, our results suggest that it would be reasonable to use the braking law of Matt et al. (2012b) over that of Réville et al. (2015a). However, some caution should be exercised when directly comparing models using the two braking laws. The model we have presented uses two fit parameters. These are the power-law indices for the source surface radius, n , and the torque scaling parameter, k . Other models that use the braking law of Matt et al. (2012b) usually have a similar torque scaling parameter to the one used in this work. However, since they do not have to model the open flux, they do not need a fit parameter like our n . Instead, these models have other free parameters. For instance, disc lifetimes are a free parameter in the work of Gallet & Bouvier (2013) and Gallet & Bouvier (2015) while the mass-loss rates used by Johnstone et al. (2015a) are specified as power laws of mass and rotation, where the power-law indices are fit parameters. Uncertainties in different models are therefore absorbed in different places making a direct comparison between models difficult. In the future, these uncertainties can be reduced through further observations of the rotation period distributions of open clusters, magnetic field strengths and disc lifetimes.

For this work, we have restricted ourselves to studying solar-mass stars on the main sequence up to the age of Sun. However, this is only one part of the lifetime of a star. In comparison to the main sequence, modelling the rotation period evolution of stars on the PMS is much more difficult. Early on, in the classical T Tauri phase, the presence of a circumstellar disc is an additional element that must be considered. Throughout the entire PMS stars spin-up as they contract towards the main sequence. However, their rotational velocities are much slower than expected from contraction alone (Vogel & Kuhi 1981) indicating that significant spin-down torques are acting on PMS stars. There is strong evidence that the presence of discs inhibits the spin-up of these stars (Edwards et al. 1993; Bouvier, Forestini & Allain 1997; Rebull, Wolff & Strom 2004) although the precise mechanism by which this is achieved is still unclear. Common suggestions include disc locking (Choi & Herbst 1996) or accretion-powered stellar winds (Matt et al. 2010, 2012a). Additionally, changes in the surface magnetic field associated with internal structure changes may also play a role (Gregory et al. 2012; Folsom et al. 2016).

In contrast to young main-sequence stars, the rotation period evolution of stars older than the age of the Sun remains relatively unconstrained. Consequently, rotation evolution models, such as the one we have presented, cannot be extended beyond the age of the Sun with any reliability. However, recent advances have allowed for the determination of rotation periods and asteroseismic ages of old field stars (García et al. 2014). These stars appear to be rotating much faster than expected from gyrochronology. Indeed, dramatically reduced braking appears to be required to explain the rapid rotation of these stars (van Saders et al. 2016). One possible explanation for such a reduction is that the nature of the dynamo changes at a Rossby number of ~ 2 such that the surface magnetic field is concentrated into smaller scales (Metcalf, Egeland & van Saders 2016). Under this interpretation, the Sun (Rossby number ~ 2) is on the verge of transitioning to a state of reduced braking. If this suggestion is true, we might expect our result, that it is

the dipole component of the magnetic field which predominantly governs the rotation evolution of main-sequence solar-mass stars, to break down at old ages. This suggestion will take time to confirm, however, since there are currently no ZDI observations of stars with Rossby numbers much bigger than 2.

In principle, the technique we have outlined in this work can also be applied to stars of other masses. However, there would be a number of additional barriers to overcome. First, more ZDI maps of saturated stars would be required. Presently, the open flux behaviour for solar-type stars in the saturated regime is relatively unconstrained in comparison to the unsaturated regime (see fig. 2b of See et al. 2017). As discussed in Section 5, for solar-mass stars, only the most rapid rotators spend any time in the saturated regime and those that do, rapidly spin-down into the unsaturated regime. Therefore, the loose constraints on the saturated level of the open flux for solar-mass stars are not a large problem. However, the critical rotation period at which saturation sets in increases for lower mass stars. This is easily seen in fig. 6 of Johnstone et al. (2015a). Consequently, the loose constraints in the saturated regime are more problematic for lower mass stars since they can spend more time in the saturated regime. Secondly, the method we have used to estimate our source surface radii is calibrated to the Sun (equation 8). Since the source surface radii of other stars are unknown, we would have nothing to calibrate to when studying the angular momentum evolution of stars with different masses. A possible method of overcoming this problem would be to recast equation (8) as $r_{ss} = \alpha P_{\text{rot}}^n$, where α is a constant of proportionality. This would, however, introduce another parameter to fit for. Finally, the magnetic properties of the very lowest masses ($<0.2 M_{\odot}$) appear to exist in one of the two states: either strong and dipolar or weak and multipolar (Morin et al. 2010). See et al. (2017) showed that the spin-down properties corresponding to these two states are very different with the instantaneous spin-down time-scales of the strong dipolar stars being two orders of magnitude shorter than their weak multipolar counterparts. As discussed by these authors, detailed angular momentum evolution modelling of these stars must wait until the number of $<0.2 M_{\odot}$ stars of known ages which have been mapped with ZDI is vastly expanded.

ACKNOWLEDGEMENTS

The authors thank an anonymous referee who helped improve the quality of this manuscript as well as Isabelle Baraffe, Sean Matt and Florian Gallet for useful discussions regarding this work. VS acknowledges support from a Science & Technology Facilities Council (STFC) post-doctoral fellowship and the European Research Council Consolidator grant AWESoMeStars. SBS and SVJ acknowledge research funding by the Deutsche Forschungsgemeinschaft (DFG) under grant SFB, project A16. RF acknowledges financial support by WOW from INAF through the Progetti Premiali funding scheme of the Italian Ministry of Education, University, and Research. This study was supported by the grant ANR 2011 Blanc SIMI5-6 020 01 ‘Toupies: Towards understanding the spin evolution of stars’ (http://ipag.osug.fr/Anr_Toupies/). This work is based on observations obtained with ESPaDOnS at the CFHT and with NARVAL at the TBL. CFHT/ESPaDOnS are operated by the National Research Council of Canada, the Institut National des Sciences de l’Univers of the Centre National de la Recherche Scientifique (INSU/CNRS) of France and the University of Hawaii, while TBL/NARVAL are operated by INSU/CNRS. We thank the CFHT and TBL staff for their help during the observations.

REFERENCES

- Altschuler M. D., Newkirk G., 1969, *Sol. Phys.*, 9, 131
 Amard L., Palacios A., Charbonnel C., Gallet F., Bouvier J., 2016, *A&A*, 587, A105
 Baraffe I., Homeier D., Allard F., Chabrier G., 2015, *A&A*, 577, A42
 Barnes S. A., 2003, *ApJ*, 586, 464
 Barnes S. A., 2007, *ApJ*, 669, 1167
 Barnes S. A., 2010, *ApJ*, 722, 222
 Barnes S. A., Weingrill J., Fritzewski D., Strassmeier K. G., Platais I., 2016, *ApJ*, 823, 16
 Blackman E. G., Owen J. E., 2016, *MNRAS*, 458, 1548
 Boro S. S., Jeffers S. V., Petit P., Marsden S., Morin J., Folsom C. P., 2015, *A&A*, 573, A17
 Boro S. S. et al., 2016, *A&A*, 594, A29
 Bouvier J., Forestini M., Allain S., 1997, *A&A*, 326, 1023
 Brown T. M., 2014, *ApJ*, 789, 101
 Brown S. F., Donati J.-F., Rees D. E., Semel M., 1991, *A&A*, 250, 463
 Choi P. I., Herbst W., 1996, *AJ*, 111, 283
 Cohen O., Drake J. J., 2014, *ApJ*, 783, 55
 Cranmer S. R., Saar S. H., 2011, *ApJ*, 741, 54
 Delorme P., Collier C. A., Hebb L., Rostron J., Lister T. A., Norton A. J., Pollacco D., West R. G., 2011, *MNRAS*, 413, 2218
 do Nascimento J.-D., Jr. et al., 2016, *ApJ*, 820, L15
 Donati J.-F., Brown S. F., 1997, *A&A*, 326, 1135
 Donati J.-F. et al., 2003a, *MNRAS*, 345, 1145
 Donati J.-F., Collier C. A., Petit P., 2003b, *MNRAS*, 345, 1187
 Donati J.-F. et al., 2006, *MNRAS*, 370, 629
 Edwards S. et al., 1993, *AJ*, 106, 372
 Fares R. et al., 2010, *MNRAS*, 406, 409
 Fares R., Moutou C., Donati J.-F., Catala C., Shkolnik E. L., Jardine M. M., Cameron A. C., Deleuil M., 2013, *MNRAS*, 435, 1451
 Folsom C. P. et al., 2016, *MNRAS*, 457, 580
 Gallet F., Bouvier J., 2013, *A&A*, 556, A36
 Gallet F., Bouvier J., 2015, *A&A*, 577, A98
 Gallet F., Charbonnel C., Amard L., Brun S., Palacios A., Mathis S., 2017, *A&A*, 597, A14
 García R. A. et al., 2014, *A&A*, 572, A34
 Garraffo C., Drake J. J., Cohen O., 2015, *ApJ*, 807, L6
 Gregory S. G., Jardine M., Collier C. A., Donati J.-F., 2006, *MNRAS*, 373, 827
 Gregory S. G., Donati J.-F., Morin J., Hussain G. A. J., Mayne N. J., Hillenbrand L. A., Jardine M., 2012, *ApJ*, 755, 97
 Guirado J. C. et al., 2010, *Astrophys. Space Sci. Proc.*, 14, 139
 Hartman J. D. et al., 2009, *ApJ*, 691, 342
 Hartman J. D., Bakos G. Á., Kovács G., Noyes R. W., 2010, *MNRAS*, 408, 475
 Irwin J., Aigrain S., Bouvier J., Hebb L., Hodgkin S., Irwin M., Moraux E., 2009, *MNRAS*, 392, 1456
 Isobe T., Feigelson E. D., Akritas M. G., Babu G. J., 1990, *ApJ*, 364, 104
 Jardine M., Collier C. A., Donati J.-F., 2002, *MNRAS*, 333, 339
 Jardine M., Vidotto A. A., See V., 2017, *MNRAS*, 465, L25
 Jeffers S. V., Petit P., Marsden S. C., Morin J., Donati J.-F., Folsom C. P., 2014, *A&A*, 569, A79
 Johnstone C. P., Jardine M., Gregory S. G., Donati J.-F., Hussain G., 2014, *MNRAS*, 437, 3202
 Johnstone C. P., Güdel M., Brott I., Lüftinger T., 2015a, *A&A*, 577, A28
 Johnstone C. P. et al., 2015b, *ApJ*, 815, L12
 Lammer H., Selsis F., Ribas I., Guinan E. F., Bauer S. J., Weiss W. W., 2003, *ApJ*, 598, L121
 Lang P., Jardine M., Donati J.-F., Morin J., Vidotto A., 2012, *MNRAS*, 424, 1077
 Lang P., Jardine M., Morin J., Donati J.-F., Jeffers S., Vidotto A. A., Fares R., 2014, *MNRAS*, 439, 2122
 Mamajek E. E., Hillenbrand L. A., 2008, *ApJ*, 687, 1264
 Matt S. P., Pinzón G., de la Reza R., Greene T. P., 2010, *ApJ*, 714, 989
 Matt S. P., Pinzón G., Greene T. P., Pudritz R. E., 2012a, *ApJ*, 745, 101

- Matt S. P., MacGregor K. B., Pinsonneault M. H., Greene T. P., 2012b, *ApJ*, 754, L26
- Matt S. P., Brun A. S., Baraffe I., Bouvier J., Chabrier G., 2015, *ApJ*, 799, L23
- Meibom S., Mathieu R. D., Stassun K. G., 2009, *ApJ*, 695, 679
- Meibom S. et al., 2011a, *ApJ*, 733, L9
- Meibom S., Mathieu R. D., Stassun K. G., Liebesny P., Saar S. H., 2011b, *ApJ*, 733, 115
- Meibom S., Barnes S. A., Platais I., Gilliland R. L., Latham D. W., Mathieu R. D., 2015, *Nature*, 517, 589
- Mestel L., Spruit H. C., 1987, *MNRAS*, 226, 57
- Metcalfe T. S., Egeland R., van Saders J., 2016, *ApJ*, 826, L2
- Morin J., Donati J.-F., Petit P., Delfosse X., Forveille T., Jardine M. M., 2010, *MNRAS*, 407, 2269
- Nicholson B. A. et al., 2016, *MNRAS*, 459, 1907
- Noyes R. W., Hartmann L. W., Baliunas S. L., Duncan D. K., Vaughan A. H., 1984, *ApJ*, 279, 763
- Pantolmos G., Matt S. P., 2017, *ApJ*, 849, 83
- Petit P. et al., 2008, *MNRAS*, 388, 80
- Pizzolato N., Maggio A., Micela G., Sciortino S., Ventura P., 2003, *A&A*, 397, 147
- Rebull L. M., Wolff S. C., Strom S. E., 2004, *AJ*, 127, 1029
- Reiners A., Mohanty S., 2012, *ApJ*, 746, 43
- Réville V., Brun A. S., Matt S. P., Strugarek A., Pinto R. F., 2015a, *ApJ*, 798, 116
- Réville V., Brun A. S., Strugarek A., Matt S. P., Bouvier J., Folsom C. P., Petit P., 2015b, *ApJ*, 814, 99
- Réville V., Folsom C. P., Strugarek A., Brun A. S., 2016, *ApJ*, 832, 145
- Ribas I. et al., 2016, *A&A*, 596, A111
- See V., Jardine M., Vidotto A. A., Petit P., Marsden S. C., Jeffers S. V., do Nascimento J. D., 2014, *A&A*, 570, A99
- See V., Jardine M., Fares R., Donati J.-F., Moutou C., 2015a, *MNRAS*, 450, 4323
- See V. et al., 2015b, *MNRAS*, 453, 4301
- See V. et al., 2016, *MNRAS*, 462, 4442
- See V. et al., 2017, *MNRAS*, 466, 1542
- Semel M., 1989, *A&A*, 225, 456
- Tu L., Johnstone C. P., Güdel M., Lammer H., 2015, *A&A*, 577, L3
- van Saders J. L., Ceillier T., Metcalfe T. S., Silva A. V., Pinsonneault M. H., García R. A., Mathur S., Davies G. R., 2016, *Nature*, 529, 181
- Vidotto A. A., Jardine M., Morin J., Donati J.-F., Lang P., Russell A. J. B., 2013, *A&A*, 557, A67
- Vidotto A. A., Jardine M., Morin J., Donati J. F., Opher M., Gombosi T. I., 2014a, *MNRAS*, 438, 1162
- Vidotto A. A. et al., 2014b, *MNRAS*, 441, 2361
- Vogel S. N., Kuhl L. V., 1981, *ApJ*, 245, 960
- Wood B. E., Müller H.-R., Redfield S., Edelman E., 2014, *ApJ*, 781, L33
- Wright N. J., Drake J. J., Mamajek E. E., Henry G. W., 2011, *ApJ*, 743, 48

APPENDIX A: DERIVING THE DIPOLAR OPEN FLUX

In this appendix, we derive the ratio of open flux to surface flux for a pure dipole mode. We remind the reader that the radial component of the magnetic field, B_r , in the PFSS model is given by

$$B_r = - \sum_{l=1}^N \sum_{m=-l}^l [la_{lm}r^{l-1} - (l+1)b_{lm}r^{-(l+2)}] P_{lm}(\cos\theta) e^{im\phi}. \quad (\text{A1})$$

From equations (4) and (5), the condition that $B_\theta(r_{ss}) = B_\phi(r_{ss}) = 0$ requires that the a_{lm} and b_{lm} coefficients obey the relation

$$a_{lm}r_{ss}^{l-1} + b_{lm}r_{ss}^{-(l+2)} = 0. \quad (\text{A2})$$

Combining equations (A1) and (A2), one finds that

$$B_r = \sum_{l=1}^N \sum_{m=-l}^l B_{lm} f_l(r) P_{lm} e^{im\phi}, \quad (\text{A3})$$

where B_{lm} and $f_l(r)$ are given by

$$B_{lm} = -a_{lm}l r_*^{l-1} + b_{lm}(l+1)r_*^{-(l+2)}, \quad (\text{A4})$$

$$f_l(r) = \left[\frac{(l+1)\tilde{r}^{-(l+2)} + l\tilde{r}_{ss}^{-(2l+1)}\tilde{r}^{l-1}}{l\tilde{r}_{ss}^{-(2l+1)} + (l+1)} \right], \quad (\text{A5})$$

where $\tilde{r} = r/r_*$ and $\tilde{r}_{ss} = r_{ss}/r_*$. For a dipole, equation (A3) therefore reduces to

$$B_r = B_{10} f_1(r) \cos\theta, \quad (\text{A6})$$

where we have chosen to use the $l=1, m=0$ mode and note that the Legendre polynomial P_{10} is given by $\cos\theta$. An identical result is obtained for the $l=1, m=1$ mode or any combination of the $l=1$ modes but we will proceed with the $l=1, m=0$ mode for convenience. In equation (A6), $f_1(r)$ is given by

$$f_1(r) = \frac{2\tilde{r}^{-3} + \tilde{r}_{ss}^{-3}}{\tilde{r}_{ss}^{-3} + 2}. \quad (\text{A7})$$

The flux at a given radial distance from the stellar surface for a pure dipole mode is therefore given by

$$\begin{aligned} \Phi_{10}(r) &= \iint_S |B_r(r)| dS \\ &= B_{10} f_1(r) r^2 \int |\cos\theta| \sin\theta d\theta \int d\phi \\ &= 2\pi B_{10} f_1(r) r^2, \end{aligned} \quad (\text{A8})$$

where S is a spherical surface of radius r . Finally, the ratio of the open flux to the surface flux for a pure dipole mode is given by

$$\frac{\Phi_{10}(r_{ss})}{\Phi_{10}(r_*)} = \frac{f_1(r_{ss})}{f_1(r_*)} \left(\frac{r_{ss}}{r_*} \right)^2. \quad (\text{A9})$$

Substituting equation (A7), one obtains

$$\frac{\Phi_{10}(r_{ss})}{\Phi_{10}(r_*)} = \frac{\Phi_{\text{open,dip}}}{\Phi_{*,\text{dip}}} = \frac{3\tilde{r}_{ss}^2}{2\tilde{r}_{ss}^3 + 1}. \quad (\text{A10})$$

This paper has been typeset from a $\text{\TeX}/\text{\LaTeX}$ file prepared by the author.